ELSEVIER

Journal of Nuclear Materials 290–293 (2001) 1040–1044

journal of nuclear materials

www.elsevier.nl/locate/jnucmat

Particle balance in NBI heated long pulse discharges on LHD

Y. Nakamura *, H. Suzuki, Y. Oka, M. Osakabe, B.J. Peterson, S. Masuzaki, T. Morisaki, J. Miyazawa, Y. Takeiri, M. Sato, T. Shimozuma, T. Mutoh, N. Noda, K. Kawahata, N. Ohyabu, O. Motojima, LHD Experimental Groups

National Institute for Fusion Science, 322-6 Oroshi-cho, Toki 509-5292, Japan

Abstract

Operational density regime of long pulse discharges heated by neutral beam injection (NBI) alone on the large helical device (LHD) is greatly extended by the replacement of stainless steel (SS) divertor plates with graphite tiles resulting in a remarkable reduction of metal impurity radiation. The plasma density can be controlled by gas puffing up to 6×10^{19} m^{-3}. Particle balance is analyzed by a global particle balance equation for helium and hydrogen discharges with high density. For helium discharges, the plasma particle inventory can be almost completely accounted for by the integrated gas puff input. A strong wall pumping is observed for hydrogen only discharges and it is found that the recycling coefficient at the start-up of the discharge is less than 0.6. The recycling coefficient increases with the wall particle inventory and approaches unity for high wall loading (23 Pa m^3). © 2001 Elsevier Science B.V. All rights reserved.

Keywords: Long pulse discharge; Particle balance; Recycling

1. Introduction

The large helical device (LHD), which is the largest superconducting machine in the world, came into operation in 1998 [1]. Since a stationary magnetic field for plasma confinement can be produced, this device is extremely suitable to study the physics and technologies for steady-state operation. Parallel with the plasma confinement study of a helical system, long pulse experiments were started by extending the pulse duration of neutral beam injection (NBI) with an injector power of 1 MW [2]. In the initial stage, the NBI heated plasma was terminated by radiative collapse due to the increase of impurities and density rise. Wall conditioning of the plasma chamber and the NBI port enabled us to extend the discharge duration and we have achieved a long pulse discharge (NBI power $P_{NBI} = 0.6$ MW, average electron denisty $\bar{n}_e = 3 \times 10^{18}$ m^{-3}, central electron temperature $T_e = 1$ keV, discharge duration $\tau_d = 21$ s) by NBI alone without great effort. However, the plasma density for long pulse operation was limited to less than 5×10^{18} m^{-3} by a relaxation oscillation phenomena (breathing), where expansion and contraction of the core plasma was repeated with a period of 1–2 s [3]. This may be caused by metal impurity accumulation due to the sputtering of stainless steel (SS) divertor plates [4]. After installation of graphite divertor tiles, no breathing plasma has been observed. As a result, the operational regime was extended up to 80 s in the discharge duration and to 6×10^{19} m^{-3} in the plasma density with a higher magnetic field of 2.75 T.

In this paper, we will focus on the long pulse discharges by NBI alone in open divertor configuration. The remarkable change of operational density regime between SS divertor plates and graphite divertor tiles will be presented (Section 3). The wall loading rate will be estimated by a global particle balance equation and the experimental results related to gas fueling and wall recycling will be presented (Section 4).

* Corresponding author. Tel.: +81-572 582 164; fax: +81-572 582 618.

E-mail address: ynakamu@lhd.nifs.ac.jp (Y. Nakamura).

PII: S0022-3115(00)00463-3

2. Experimental arrangement and diagnostics

The plasma experiments on LHD have been started in an open divertor configuration with a SS inner wall, which was actively cooled by water for the capability of steady-state operation with an injection power of 3 MW. For the third experimental campaign, a large number of graphite divertor plates have been installed at the strike points of four divertor legs, which rotate helically around the torus. The divertor plates were fixed to SS cooling pipes through copper heat sinks. The heat removal capability was 0.3 MW/m^2, i.e., 3 MW of conducted power. The plasma vessel wall and the divertor plates have been conditioned by discharge cleaning of helium (or hydrogen) glow (filling pressure ~1 Pa, wall temperature 30°C, discharge duration 8 h) or electron cyclotron resonance (ECR heating with the frequency of 2.45 GHz) plasmas every night. Titanium gettering has been carried out in the latter half of the experimental campaign covering approximately 20–30% of the vacuum vessel surface. At present, LHD has an open divertor configuration and no active pumping system.

The pressure of plasma chamber was measured by a fast-time-response ionization gauge located in the upper port near the horizontal port for pumping. The amount of gas input from the neutral beam line was estimated by monitoring the pressure at the end of the beam drift tube. Data for the calculation of the particle balance were obtained from calibrated gas valves, far-infrared (FIR) interferometer data for the plasma density, and neutral beam power which gives the beam fueling rate. Radiation profiles were measured by arrays of resistive metal foil bolometers which view the plasma from vertical and horizontal diagnostic ports.

3. Operational density regime in long pulse discharge

First of all, we present a remarkable change of operational density regime between long pulse discharges with SS divertor plates and with graphite divertor tiles. Fig. 1 shows the dependence of the fraction of radiated power on the line integrated electron density. In the second experimental campaign, since the machine had no graphite tiles to bear the divertor particle and heat flux, the radiation power rapidly increased with the density because of the high concentration of metal impurities (mainly iron) most likely due to the sputtering of SS divertor plates. In these discharges, the metal impurities accumulated in the plasma core and the core radiation was clearly observed as shown in Fig. 2(a), where a radiation profile for helium discharge with SS divertor plates is indicated. When the density was increased, there occurred a relaxation oscillation phenomena (breathing), where expansion and contraction of the core plasma was repeated with a period of 1–2 s. As a result, the plasma density in long pulse operation was limited to less than 10^{19} m^{-3}. This limitation can be evaluated by global power balance. When the total radiation increases with the density and when it reaches to about 85% of deposited heating power, a minor radiative collapse due to the light impurities (C, O) occurs in

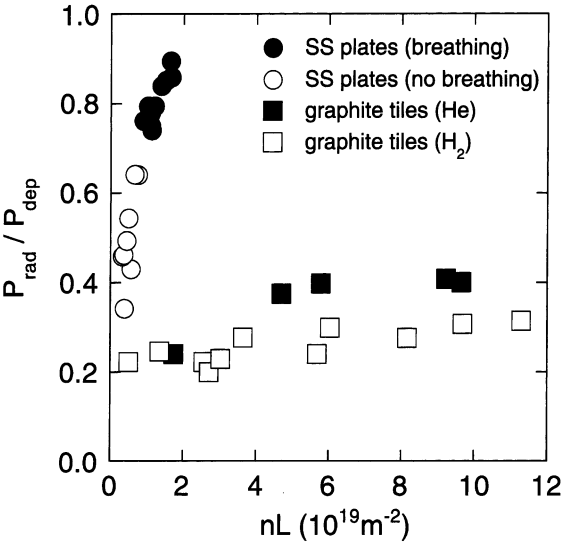

Fig. 1. Change of the fraction of radiated power with the line integrated electron density. The deposited power (P_{dep}) was calculated from the shine-through NBI power. The line integrated electron density ($nL = \bar{n}_e L_{FIR}$, L_{FIR} is the chord length of FIR interferometer) is measured by FIR interferometer. The low-density discharges (solid and open circles) were performed with $R = 3.75$ m and $B = 1.5$ T ($L_{FIR} = 1.6$ m). The solid squares indicate the discharges with $R = 3.75$ m and $B = 1.5$ T and the open squares with $R = 3.6$ m and $B = 2.75$ T ($L_{FIR} = 1.8$ m).

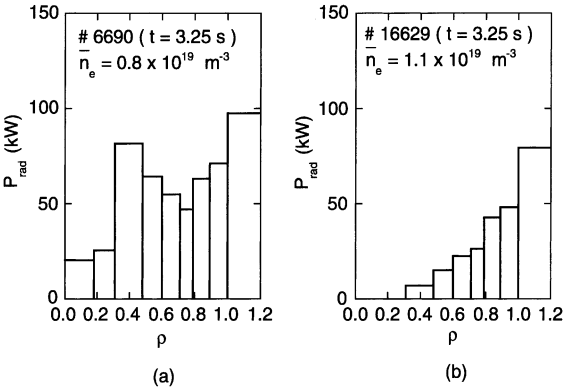

Fig. 2. Radiation profiles for the discharges with: (a) SS divertor plates; (b) graphite tiles. In the case of SS plates, the strong radiation in the plasma core was caused by the metal impurities.

the peripheral region and the hot plasma core contracts. After installation of graphite tiles along the divertor legs, no breathing plasma has been observed even in the same magnetic configuration ($R = 3.75$ m, $B = 1.5$ T). Then a remarkable reduction of core radiation was observed as shown in Fig. 2(b), where a radiation profile for hydrogen discharge with graphite tiles is depicted. Moreover, the long duration plasmas revealed a new feature on the density dependence of the fraction of radiated power. The radiation loss increased with the density up to 3.5×10^{19} m^{-3} and remained constant there. The saturated level was 40% for helium discharges in the magnetic configuration of $R = 3.75$ m and $B = 1.5$ T. The same density dependence was also observed for hydrogen discharges in the different magnetic configuration ($R = 3.6$ m, $B = 2.75$ T). The saturated level was about 30% lower than that for helium discharges. This difference can be attributed to the magnetic configuration and strong magnetic field. In this way, we have achieved a long pulse discharge with a high density of 6×10^{19} m^{-3} and the plasma density can be controlled by external gas puffing.

4. Global particle balance

4.1. Wall loading during long pulse discharges

Here we investigate global particle balance in high-density long pulse discharges by estimating the difference between the input gas sources and sinks. The wall particle loading rate during the discharge can be described by

$$\Gamma_{\mathrm{wall}} = \Gamma_{\mathrm{gas}} + \Gamma_{\mathrm{NBI}} + \Gamma_{\mathrm{NBI}}^{\mathrm{gas}} - \frac{\mathrm{d}N_{\mathrm{p}}}{\mathrm{d}t} - \frac{\mathrm{d}N_0}{\mathrm{d}t} - \Gamma_{\mathrm{pump}}, \qquad (1)$$

where Γ_{gas} is the gas puff fuelling rate, Γ_{NBI} the energetic beam particle fuelling rate, $\Gamma_{\mathrm{NBI}}^{\mathrm{gas}}$ the cold particle fuelling rate from gas in the beam line, $\mathrm{d}N_{\mathrm{p}}/\mathrm{d}t$ the neutral loss rate due to plasma formation, $\mathrm{d}N_0/\mathrm{d}t$ the neutral gas build-up rate and Γ_{pump} is the pump exhaust rate. This type of particle balance has been used for many tokamak discharges [5]. Γ_{NBI} was measured from the beam energy and deposited power and $\Gamma_{\mathrm{NBI}}^{\mathrm{gas}}$ from the gas flow through the beam duct by monitoring the pressure at the end of the beam drift tube. The neutral loss rate due to plasma formation was estimated as the rate of change in plasma inventory. In this analysis, we assume $Z_{\mathrm{eff}} = 1$ and flat density profiles typical of LHD discharges. With these assumptions, the plasma inventory is roughly equal to the electron inventory, which can be estimated as the product of the volume averaged electron density and the plasma volume (V_{p}), i.e. ($N_{\mathrm{p}} \approx N_{\mathrm{e}} \approx \overline{n}_{\mathrm{e}} V_{\mathrm{p}}$). In addition, neutral gas build-up was taken into account by assuming that the neutral pressure in the plasma vacuum vessel was homogeneous. The particle exhaust ($\Gamma_{\mathrm{pump}} = S_0 P_0$) with a usual pumping system, which consists of four turbomolecular pumps (13 m^3/s) and two cryopumps (86 m^3/s), was estimated from the pumping speed ($S_0 = 67$ m^3/s) and the neutral pressure (P_0) near the pumping duct. The contribution of the last two terms to the particle balance was found to be less than 10% of gas puff rate [6]. The net wall loading over the duration of the discharge is readily obtained by the integration of the wall loading rate (Γ_{wall}). The components of the particle balance described by Eq. (1) are shown in Figs. 3 and 4 for helium and hydrogen discharges, respectively, with flow rates in Pa m^3/s on the left-hand ordinates and integrated particle numbers in Pa m^3 on the right-hand ordinates. In both the discharges, the plasma density was kept constant ($\overline{n}_{\mathrm{e}} \approx 4 \times 10^{19}$ m^{-3}) by a gas puff system with a feedback loop. It is clear that there is a great difference in wall pumping between helium and hydrogen discharges. In helium discharges, the plasma density was built up by the gas puffing and the resulting plasma inventory was almost the same as the integrated gas input. In addition, the gas puff was not required after the density build-up phase. The wall was only loaded by the particle input ($\Gamma_{\mathrm{NBI}}^{T} = \Gamma_{\mathrm{NBI}} + \Gamma_{\mathrm{NBI}}^{\mathrm{gas}}$) from the NBI system. On the other hand, the gas required during the density build-up was significantly higher for hydrogen discharges, and the gas puff with the rate of about 1.2 Pa m^3/s was needed to maintain the density. Most of the input gas was absorbed by the wall and the wall inventory showed a net

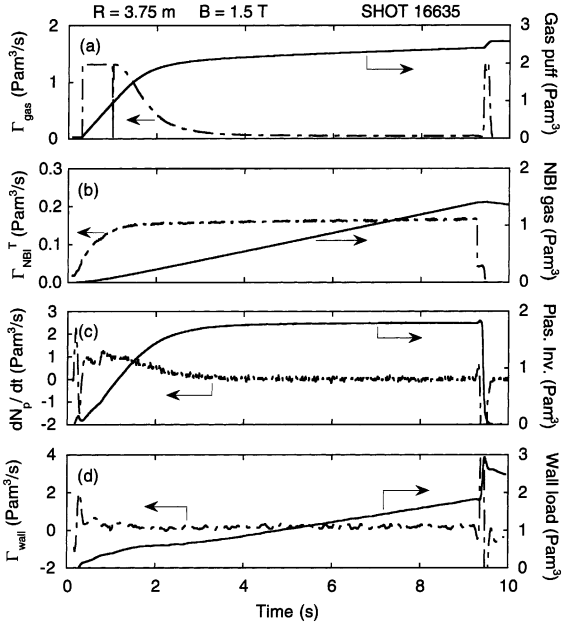

Fig. 3. Particle balance for helium discharge: (a) gas puff; (b) fueling by NBI; (c) plasma inventory; (d) inferred wall load.

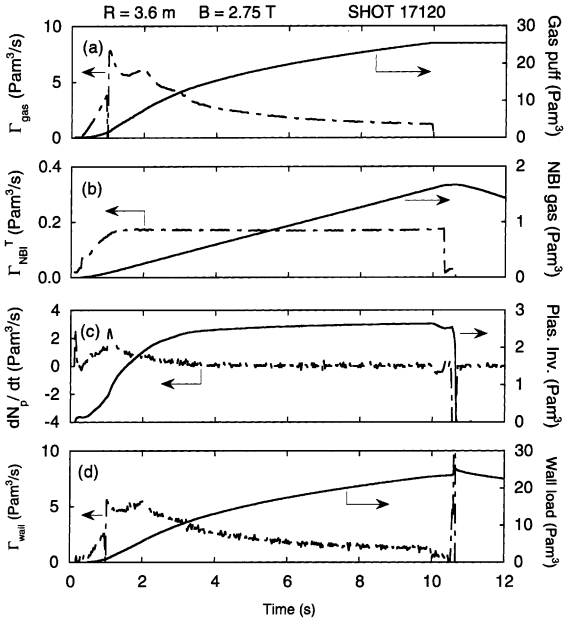

Fig. 4. Particle balance for hydrogen discharge: (a) gas puff; (b) fueling by NBI; (c) plasma inventory; (d) inferred wall load.

increase of 23 Pa m^3/s at the end of the discharge. It is evident that the wall pumping was strong in the plasma build-up phase and still effective at the end of the discharge.

4.2. Fueling and wall recycling properties

In order to study fueling and wall recycling properties, a series of discharges was carried out with a common format. The discharges were initiated with a small pre-puff and electron cyclotron heating (ECH) resulting in a very low-density target plasma. After plasma breakdown, gas puffing with constant flow rates between 0.6 and 9 Pa m^3/s was applied at the same time of NBI and a ramp-up rate of the plasma inventory was observed. The gas puffing lasted for 3–8 s and a density decay after the termination of the gas puff was also investigated. From the above evaluation for particle balance, the change of plasma inventory is approximately described by

$$\frac{dN_p}{dt} = \eta\Gamma_{gas} - \frac{N_p}{\tau_p} + R\left\{(1-\eta)\Gamma_{gas} + \frac{N_p}{\tau_p}\right\} = \{\eta + R(1-\eta)\}\Gamma_{gas} - \frac{N_p}{\tau_p^*} \quad (2)$$

considering only the external gas puffing as the gas input and neglecting the exhausting term and the neutral gas build-up. Here η is the fueling efficiency, τ_p the particle confinement time, R the recycling coefficient to the core plasma, and $\tau_p^* = \tau_p/(1-R)$ is the global particle confinement time. In this model, since it is difficult to distinguish between plasma shielding effect and wall recycling effect, η is assumed to be constant and R depends on the wall recycling only. Accordingly, the rising rate of plasma inventory due to the constant gas puff gives information on the wall pumping state at the start-up phase of the discharge. Fig. 5 shows the relation between the gas puff rate and the ramp-up rate of plasma inventory. In comparison, data for helium discharges with the short gas puffing (0.6 s) are also plotted in Fig. 5. For helium discharges, the ramp-up rate of plasma inventory is quite close to the gas puff rate. This means that $\eta + R(1-\eta) \cong 1$, i.e., $R \cong 1$, while the proportional coefficient is about 0.6 for hydrogen discharges. It leads to $R \leqslant 0.6$ since $\eta + R(1-\eta) \geq R$ for all η values ($0 \leqslant \eta \leqslant 1$). Therefore, in this experimental series, it was found that the wall condition was always in a strong pumping state before the discharge. This is due to the desorption of gas deposited at the wall surface during the interval between two NBI shots. In fact, the gas pumped for the interval was almost the same as the injected one. On the other hand, the decay time τ_p^* of the plasma inventory after the termination of the gas puff gives information on the wall recycling after gas puffing. Fig. 6 shows the dependence of the decay rate of the plasma inventory on the wall inventory, which is evaluated by the global particle balance in Eq. (1). τ_p^* increased with the wall loading and reached 5.5 s for the wall inventory of 23 Pa m^3/s. In comparison, τ_p^* was more than 15 s for helium discharges. The τ_p^* values do

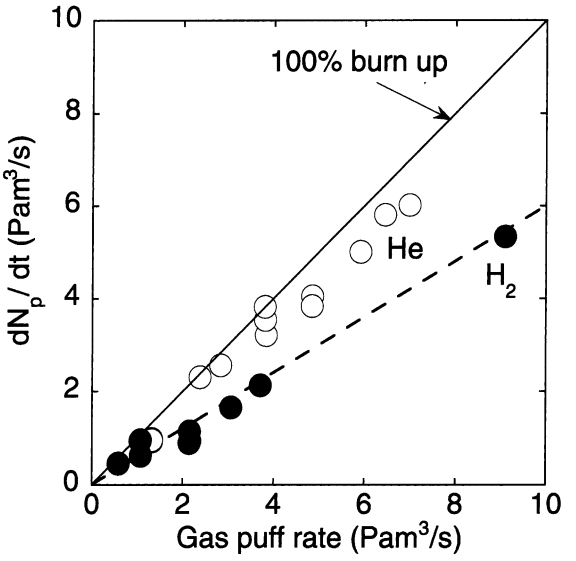

Fig. 5. Relationship between the gas puff rate and the ramp-up rate of plasma inventory for helium and hydrogen discharges.

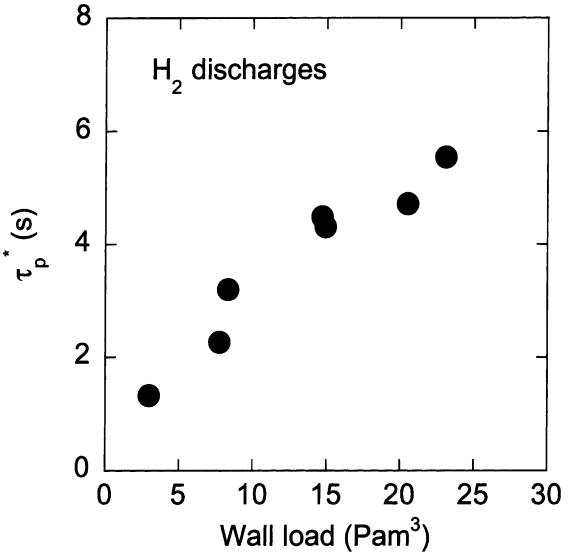

Fig. 6. Dependence of the global particle confinement time (τ_p^*) on the wall inventory.

not directly reflect the wall state, because they contain τ_p which depends on the density and its profile. However, the fact that the wall recycling increased with the wall loading does not change. For example, $\tau_p^* = 5$ s leads to $R = 0.96$, assuming that $\tau_p = 0.3$ s is close to the energy confinement time. The global recycling coefficient increases and approaches unity by a high-density discharge and a long pulse discharge. However, the evidence of complete wall saturation (a positive slope of the fueling rate) has not been observed for hydrogen discharges within the total gas input of 27 Pa m^3. A similar result has been obtained in long pulse discharges in Tore Supra[7–9]. In these experiments, it was shown that no wall effect was observed for helium discharges and there was a dominant role of the wall for deuterium discharges [8]. Moreover, the wall particle inventory was estimated from shot to shot by a balance of the injected and pumped gas, and it was found that the wall changed from a deeply desaturated state to a saturated one on increasing the wall inventory [9]. Since the gas input in our experiment is still less than the global amount of deposited gas (70 Pa m^3) in Tore Supra, further experiments with a large amount of gas input will be required to observe the wall saturation.

5. Conclusions

In NBI heated long pulse discharges on LHD, there was a great difference in radiation between discharges with SS divertor plates and graphite tiles. Installation of graphite tiles yielded a remarkable reduction of metal impurities and radiated power. The operational density regime was extended to a large extent ($\overline{n}_e \cong 6 \times 10^{19}$ m^{-3}). Global particle balance was investigated comparing helium and hydrogen discharges. Only for hydrogen discharges, the wall pumping played an important role in maintaining a constant plasma density. From experiments with constant gas puffing, it was found that the global recycling coefficient before the discharge was less than 0.6 for hydrogen. The recycling coefficient increased with the wall inventory and approached unity. However, the wall provides sufficient particle pumping even after the high wall loading (23 Pa m^3).

Acknowledgements

The authors thank Professor M. Fujiwara (director of NIFS) and Professor A. Iiyoshi (former director of NIFS) for their continuous guidance and encouragement.

References

[1] O. Motojima, et al., Phys. Plasma 6 (1999) 1843.
[2] Y. Takeiri, N. Noda, Y. Nakamura, et al., Rev. Sci. Instrum. 70 (1999) 4260.
[3] Y. Takeiri, Y. Nakamura, et al., Plasma Phys. Control Fus. 42 (2000) 147.
[4] B.J. Peterson et al., J. Plasma Fus. Res., Series 3 (2000).
[5] R. Maingi, et al., Nucl. Fus. 36 (1996) 245.
[6] Y. Nakamura et al., J. Plasma Fus. Res., Series 3 (2000).
[7] D. Van Houtte, et al., Nucl. Fus. 33 (1993) 137.
[8] T. Loarer, et al., Plasma Phys. Control Fus. 37 (1995) A203.
[9] C. Grisolia, et al., J. Nucl. Mater. 196–198 (1992) 281.